Evidence for Precursors of the Coronal Hole Jets in Solar Bright Points

Salome R. Bagashvili[1,3,4] , Bidzina M. Shergelashvili[2,3,4] , Darejan R. Japaridze[3], Vasil Kukhianidze[3], Stefaan Poedts[1] ,
Teimuraz V. Zaqarashvili[2,3,5] , Maxim L. Khodachenko[2] , and Patrick De Causmaecker[4]

[1] Center for Mathematical Plasma Astrophysics, Department of Mathematics, KU Leuven, 200 B, B-3001 Leuven, Belgium
[2] Space Research Institute, Austrian Academy of Sciences, Schmiedlstrasse 6, A-8042 Graz, Austria; Bidzina.Shergelashvili@oeaw.ac.at
[3] Abastumani Astrophysical Observatory at Ilia State University, Kakutsa Cholokashvili Ave 3/5, 0162 Tbilisi, Georgia
[4] Combinatorial Optimization and Decision Support, KU Leuven Campus Kortrijk, E. Sabbelaan 53, B-8500 Kortrijk, Belgium
[5] Institute of Physics, IGAM, University of Graz, Universitätsplatz 5, A-8010 Graz, Austria

Abstract

A set of 23 observations of coronal jet events that occurred in coronal bright points has been analyzed. The focus was on the temporal evolution of the mean brightness before and during coronal jet events. In the absolute majority of the cases either single or recurrent coronal jets (CJs) were preceded by slight precursor disturbances observed in the mean intensity curves. The key conclusion is that we were able to detect quasi-periodical oscillations with characteristic periods from sub-minute up to 3–4 minute values in the bright point brightness that precedes the jets. Our basic claim is that along with the conventionally accepted scenario of bright-point evolution through new magnetic flux emergence and its reconnection with the initial structure of the bright point and the coronal hole, certain magnetohydrodynamic (MHD) oscillatory and wavelike motions can be excited and these can take an important place in the observed dynamics. These quasi-oscillatory phenomena might play the role of links between different epochs of the coronal jet ignition and evolution. They can be an indication of the MHD wave excitation processes due to the system entropy variations, density variations, or shear flows. It is very likely a sharp outflow velocity transverse gradients at the edges between the open and closed field line regions. We suppose that magnetic reconnections can be the source of MHD waves due to impulsive generation or rapid temperature variations, and shear flow driven nonmodel MHD wave evolution (self-heating and/or overreflection mechanisms).

Key words: methods: data analysis – methods: observational – methods: statistical – Sun: corona – Sun: magnetic fields

1. Introduction

Coronal jets (CJs) are collimated plasma flows observed in extreme ultraviolet (EUV), X-Rays, and white-light images across the entire solar atmosphere: in quiet corona and active regions (Schmieder et al. 2013; Guo et al. 2014; Raouafi et al. 2016; Chandra et al. 2017) and in coronal holes (CHs) (Young & Muglach 2014a, 2014b; Sterling et al. 2015; Young 2015). The contemporary space-based observational missions (such as *Hinode*, *Solar Dynamics Observatory*, and others) with state-of-the-art spatiotemporal resolution revealed that jetlike transient processes occur very often in the solar atmosphere (Savcheva et al. 2007; Paraschiv et al. 2010).

Despite some observational and theoretical studies (Shibata et al. 1992; Yokoyama & Shibata 1995; Shimojo et al. 2001; Ryutova et al. 2008; Pariat et al. 2009; Archontis et al. 2010; Magara 2010; Moore et al. 2010; Pariat et al. 2010), the mechanism for CJ formation and evolution is not entirely understood. There is a general consensus that all of the jetlike features should originate from the common basic formation mechanism, namely, the release of free magnetic energy due to magnetic reconnection processes (Shibata et al. 2007; Pariat et al. 2009). The majority of the investigated CJs eject from newly emerging or developed bright points (BPs; Nisticò et al. 2009) during the peak of their brightness (Pucci et al. 2012). In the past, BPs visible in Hα and in EUV have been frequently observed before cool jets called surges and collimated with EUV jets (Gu et al. 1994; Canfield et al. 1996; Schmieder et al. 1996). Sterling et al. (2015, 2016) presented new results that suggest that mini-filament eruptions trigger

CJs, and there might be no difference in the scenario of standard and blowout jet formation. Furthermore, Panesar et al. (2016) presented an observational study that reports that mini-filament eruptions, which lead to CJ acceleration, are driven by flux cancelation in the photosphere.

The matter of our focus, in this Letter, is a particular aspect of the observed dynamics, namely, a systematic observational study of the CJs associated with on-disk CHs. Our aim was to deduce from the extreme EUV data analysis the character of the temporal behavior of the mean intensity and the connection to the jet outflow processes themselves.

In general, recent studies report on the BP brightness fluctuations and a variety of their oscillation periods (Nolte et al. 1979; Sheeley & Golub 1979; Strong et al. 1992; Mandrini et al. 1996; Aulanier et al. 2007; Tian et al. 2008; Kumar et al. 2011; Pontin et al. 2011; Guo et al. 2013; Schmieder et al. 2013). Besides, Pucci et al. (2012) followed the BP brightness evolution for several CJs and found that most of the jets occurred in close temporal association with the brightness maxima. This observational evidence leads us to the assumption that in the dynamics of BPs, different magnetohydrodynamic (MHD) wavelike or oscillatory disturbances may take place. In this regard, Pariat et al. (2012) assume that the observed structure of CJs could be explained using the generation of a helical kinklike wave. Lee et al. (2015) report that jets manifest oscillatory motions during their ejection linking them to wave processes. Moreover, such disturbances may provide a link for the coupling of the dynamic processes occurring in BPs. It is natural to assume (in the current study only at an intuitive level) that these wavelike processes can
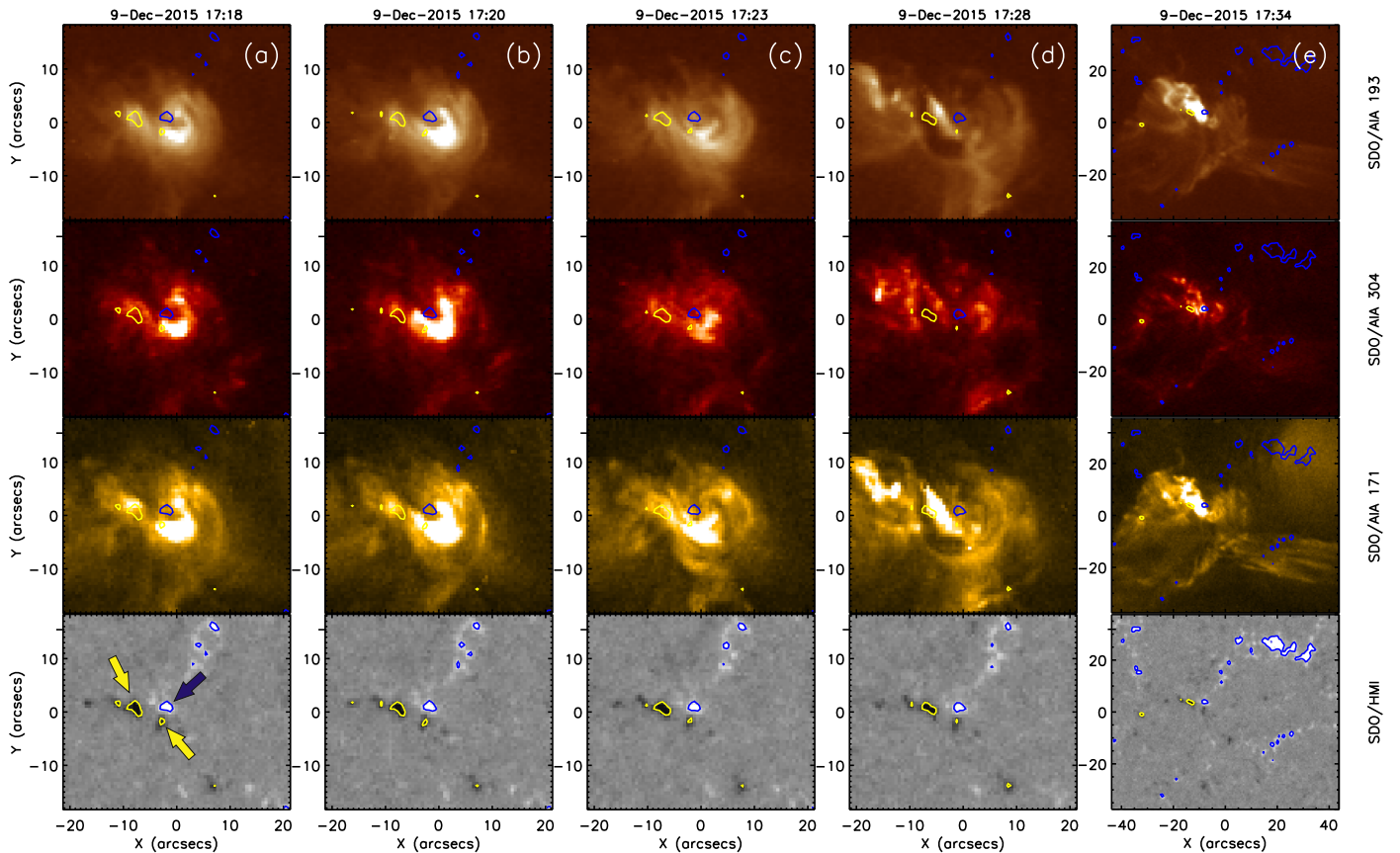
Figure 1. Sample BP before and during CJ ejection process. The top three rows represent overlap of *SDO*/AIA 193, 304, and 171 Å intensity images and *SDO*/HMI photospheric magnetograms. The bottom row represents HMI magnetogram separately. Blue and yellow contours indicate positive and negative magnetic field polarities, respectively. These regions are also indicated with arrows in the bottom row of panel (a). Panel (a): the beginning of precursor; panel (b): the peak of the precursor brightening; panel (c): the time after the precursor when still there is no signature of main jet outflow; panel (d): the moment when the structure is destabilized and the jet-type instability starts; panel (e): the fully developed transient jet outflow. In panel (e), we take a wider observational window as shown on the corresponding axes.

be excited in the substantially nonequilibrium environment such as shear flows (Shergelashvili et al. 2006) or flows with thermal variations (Shergelashvili et al. 2007). These kinds of disturbances can be excited in the vicinity of and triggered by the aforementioned, conventionally accepted coronal jet energy sources, namely, magnetic reconnection and flux emergence/cancelation processes. For analytical modeling under these frameworks, one should keep in mind that such wavelike dynamical processes follow more or less similar scenarios: ignition of a precursor disturbance, its evolution in time, and triggering of a main larger event. Besides, the overall contribution of CJ incidents in the energy budget of the solar atmosphere and wind can be estimated using the statistical properties of CHs reported by Bagashvili et al. (2017), with which the BPs of interest can be linked. However, before achieving such far-reaching consequences regarding analytical modeling, a thorough observational analysis and confirmation of the regular presence of such quasi-oscillatory type of precursors are needed. These are the ultimate goals of the observational studies reported in the current Letter.

2. The Methodology of Observations and Data Analysis

We used data from the Atmospheric Imaging Assembly (AIA) on board of the *Solar Dynamic Observatory* (*SDO*; Lemen et al. 2012), which monitors the Sun with 0.6″ spatial

and 12 s temporal resolution (Boerner et al. 2012). The *SDO*/AIA data are retrieved, processed, and analyzed using standard procedures with the SolarSoft (SSW) package. Our particular interest goes to BPs and CJs situated within and at the edges of the CHs. The CHs have been chosen from different areas of both hemispheres, excluding regions very close to limbs, during the period from 2015 December 1 until 2016 May 1. In total, we investigated 23 (spatiotemporally independent) CJs using *SDO*/AIA 193 Å channel images. Among them were recurrent jets, which, nonetheless, we treated each jet phenomenon as a separate event.

For despiking, bad pixel/cosmic-ray influence correction and flat-fielding, level 1 data has been processed into level 1.5 using the aia_prep.pro code. From the obtained files, we cut out rectangular boxes for each event and create their time series. We applied the rot_xy procedure to exclude the solar rotation effect. Figure 1 shows several example snapshots from such an image sequence. The images are created using the AIA 193, 304, and 171 Å channel data both in combination with HMI photospheric magnetograms. Blue and yellow contours indicate positive and negative magnetic field polarities, respectively. In the middle (small yellow and blue closed contours) of the BP there is a small bipolar closed magnetic structure anchored in the photosphere and extended in the form of a magnetic loop through the base of the solar corona. Besides, it is seen that the footpoints of the central loop are surrounded by a system of
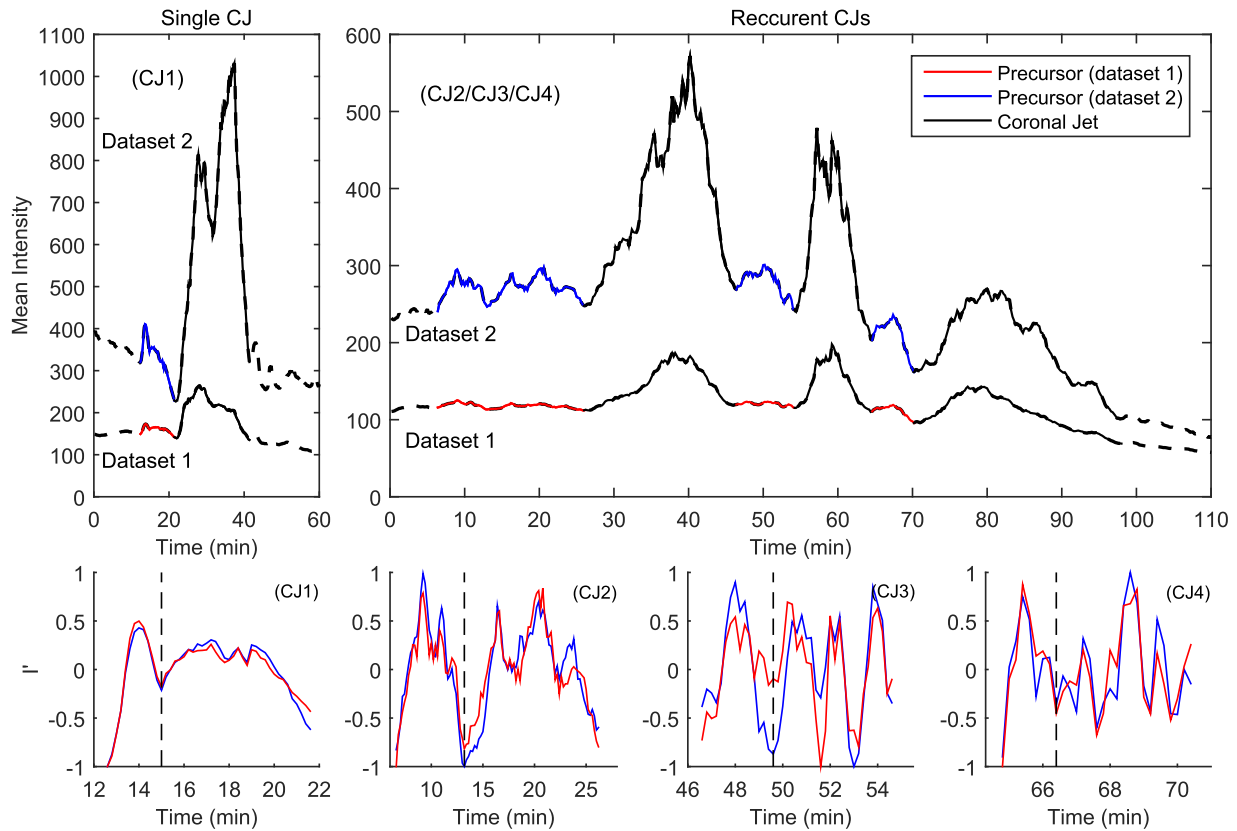
Figure 2. Coronal jet intensity curves for data set 1 (without threshold—bottom curves) and data set 2 (with threshold—top curves) in the top panels (CJ1) and (CJ2/CJ3/CJ4). Red (data set 1) and blue (data set 2) solid-line parts of the curves indicate precursors events. Accordingly, we plot zooms of these parts in the detrended form in the bottom panels (CJ1), (CJ2), (CJ3), and (CJ4), respectively. Panels (CJ1; top and bottom) correspond to the case of the single CJ that started at 2015 December 9 17:28 UT with a precursor start approximately 9.8 minutes before the CJ release. While panels (CJ2/CJ3/CJ4), (CJ2), (CJ3), and (CJ4) demonstrate the case of the recurrent CJs that started at 2015 December 30 23:16 UT, which includes three subsequent plasma ejections. Each of them has precursors starting 19.6, 7.8, and 5.6 minutes before the respective CJs. Vertical dashed lines represent the end of precursor ignition.

magnetic field concentration areas (edge of supergranules) in the chromospheric network. These magnetic flux concentration regions are closely situated to each other and are also embedded in the global CH magnetic field of positive polarity (Figure 1). Panel (a) shows the beginning of the precursor for each wavelength and for the magnetogram as well; panel (b) corresponds to the peak of the precursor brightening; panel (c) corresponds to the time after the precursor when there is still no signature of the main jet outflow; panel (d) demonstrates the moment when the structure is destabilized and the jet-type instability starts and filamentary darkening aside the BP loop appears, just like in many similar observations; panel (e) corresponds to the fully developed transient jet outflow.

In order to perform a rigorous analysis on the observed dynamical processes, we created two types of 193 Å intensity curves in Figure 2. The first type of data (data set 1) comprises the calculation of the mean intensity values of the entire cutout BP-boxes. The second type of data (data set 2) is created using the average over all pixels of modified intensity value cutout BP-boxes obtained through noise deduction (using the methodology similar to the one outlined in Chandrashekhar et al. 2013). The final values in data set 2 exclude low-intensity noise containing regions of BP-boxes. Consequently, in data set 2, the effect of background noise is removed and all the transient disturbances are more sharply observable. All 23 BPs and corresponding jets we investigated have more or less similar morphological and dynamical properties. Examples of

brightness evolution curves are shown in the top panels (CJ1) and (CJ2/CJ3/CJ4) of Figure 2.

Despite the fact that the examples of the BPs we studied show the structure and dynamics conventionally standardized in the related literature (Sterling et al. 2015; Raouafi et al. 2016), our study uncovers the systematic presence of relatively low amplitude (compared to the jets) quasi-oscillatory dynamic processes before each main jet event (the solid-line, black parts of the curves in the top panels (CJ1) and (CJ2/CJ3/CJ4) of Figure 2. We argue that these processes can represent precursors of jets (the solid-line, red and blue colored parts of the curves in the top panels (CJ1) and (CJ2/CJ3/CJ4) of Figure 2. Further, we plot these precursor parts zoomed in and detrended for an isolated single (top panel (CJ1)) and for a recurrent jet event (panels (CJ2), (CJ3), and (CJ4)). The corresponding FFT periodograms are presented in Figure 3. It is apparent that regardless of the type of the event (single or recurrent) the quasi-oscillatory variation of the mean intensity of precursors is systematically observed.

3. Analysis of the Results

Our first finding is that in the absolute majority of instances (20 out of 23) we detect a characteristic brightening of the observed BP preceding, by a few minutes, the main jet outflows. We consider these processes as CJ precursors (as shown in Figure 2). In this Letter, we show only illustrative
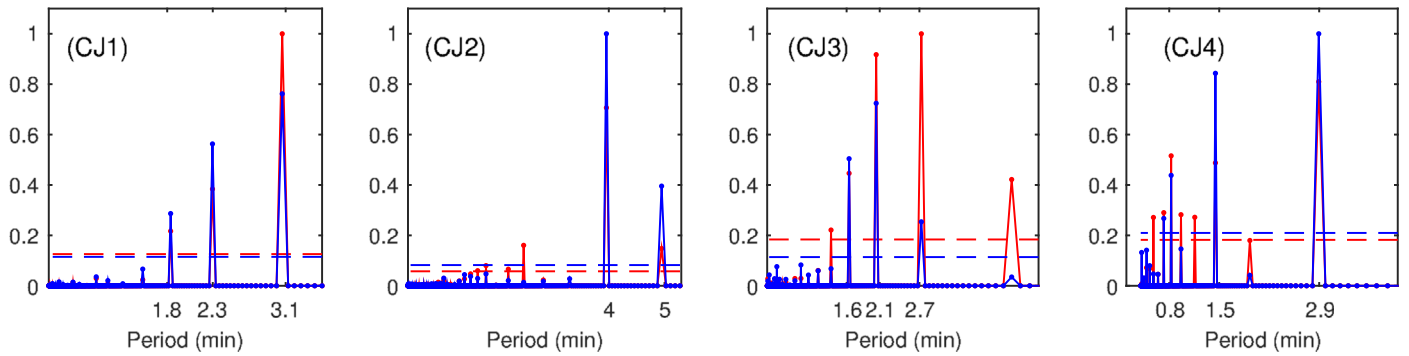
Figure 3. Set of calculated FFT periodograms accordingly corresponding to cases shown in the bottom panels (CJ1), (CJ2), (CJ3), and (CJ4) of Figure 2. The coloring is the same as in Figure 2, and horizontal blue and red dashed lines represent 95% confidence levels for data set 2 and data set 1, respectively. The spectral powers are normalized on the maximum power pick shown in each panel.

Table 1
Parameters of CJs and Their Precursors

No.	Obs. Start Time	Location	Type	τ_{PI}	τ_{PT}	τ_{CJ}	$\Delta\tau_{Peaks}$	Osc. Periods
CJ1	2015 Dec 09 17:18	355, −260	S	1.75/1.28	9.4/9.8	7.16/8.13	13.55/14.49	1.8–3.1
CJ2	2015 Dec 30 22:56	−780, −270	R	4.58/4.78	19.6/19.6	9.20/10.15	13.83/13.31	4.0–5.0
CJ3	2015 Dec 30 23:40	−780, −270	R	2.78/2.27	7.8/7.8	4.85/5.54	8.03/8.02	1.6–2.7
CJ4	2015 Dec 30 23:58	−780, −270	R	2.59/1.51	5.6 /5.6	16.38/16.96	13.11/12.59	0.7–2.9
CJ5	2015 Dec 31 02:12	−770, −280	R	4.40/3.86	13.6/13	11.77/11.33	20.78/20.95	1.4–4.6
CJ6	2015 Dec 31 02:52	−770, −280	R	2.97/3.05	8/8	6.23/5.96	14.27/14.14	0.9–3.4
CJ7	2015 Dec 07 15:56	385, 510	R	13.82/12.72	21.2/20	13.49/15.60	20.64/23.80	1.9–5.1
CJ8	2015 Dec 07 17:08	385, 510	R	3.17/3.85	4.9/5.4	8.05/8.24	9.49/8.96	1.2–2.1
CJ9	2015 Dec 08 11:38	15, −225	S	4.73/5.03	20 /20.2	6.38/4.42	19.92/19.43	2.3–4.1
CJ10	2015 Dec 05 09:11	430, 230	S	1.72/1.62	2.2/2.2	9.21/8.43	5.71/6.50	0.5–1.2
CJ11	2015 Dec 10 19:25	765, −230	R	5.79/6.09	14.6/13.8	5.64/6.50	15.39/15.57	1.2–3.7
CJ12	2015 Dec 10 21:04	765, −235	R	5.90/5.91	7.8/7.8	10.77/10.52	11.05/11.58	1.0–4.0
CJ13	2016 Mar 21 21:30	515, 585	S	12.02/12.59	12.59/12.59	12.02/12.59	0/0	…
CJ14	2016 Mar 21 21:21	630, 435	S	6.73/6.49	11.6/10.4	11.80/11.51	11.45/12.46	0.8–1.9
CJ15	2016 Mar 22 02:40	−705, −130	R	3.57/4.05	4.05/4.05	3.57/4.05	0/0	…
CJ16	2016 Mar 22 02:55	−660, −80	R	9.44/9.06	9.06/9.06	9.44/9.06	0/0	…
CJ17	2016 Apr 18 10:44	−460, 275	S	1.86/1.89	3.2/3.2	3.36/3.32	3.24/3.15	0.4–1.7
CJ18	2016 Apr 18 13:39	−550, 445	S	2.70/2.22	4.4/3.4	10.40/9.96	8.99/10.37	0.9–1.5
CJ19	2016 Apr 18 14:08	−520, 385	S	0.93/0.88	2/2.2	6.28/5.42	9.12/8.81	0.8–1.2
CJ20	2016 Apr 18 16:58	605, 460	R	3.77/3.34	4/6.0	9.87/10.35	17.59/17.05	0.5–2.1
CJ21	2016 Apr 18 21:25	640, 450	R	1.81/2.36	3.2/3.2	6.35/5.99	6.40/6.15	0.5–1.1
CJ22	2016 Apr 18 21:57	640, 450	R	1.90/1.90	2.4/2.4	6.39/5.81	5.28/5.34	0.5–0.6
CJ23	2016 Apr 18 18:25	−485, 385	S	3.03/3.08	6.2/6.6	6.12/4.91	8.54/8.27	1.8–3.6

Note. Complete set of 23 selected CJ and corresponding precursor parameters. Location represents BP (x, y) coordinates in arcsecs; in the column Type we have two possible values S—single and R—recurrent; τ_{PI} represents the precursor ignition duration; τ_{PT} is the precursor total evolution time span; (τ_{CJ})—CJ durations, $\Delta\tau_{Peaks}$—the time intervals between precursor and CJ peaks; Osc. Periods shows the minimum and maximum values of precursor oscillation periods. The parameters having time dimension are measured in minutes.

examples of single and recurrent jet events and the full analysis all 23 jets will be given on our project website.

Figure 2 shows only illustrative examples of single (top panel (CJ1)) and recurrent (panel (CJ2/CJ3/CJ4)) jet events (out of all 23 investigated cases). The enhancement of the BP intensity is visible several minutes before the CJ ejection in the case of both data set 1 and data set 2 mean intensity curves. In both cases of single and recurrent jets, the precursors are systematically observed before each plasma ejection. In the top panel (CJ1) of Figure 2, the existence of the precursor of the single jet event is evident (2015 December 9 17:18 UT). Besides, the set of recurrent events in panel (CJ2/CJ3/CJ4) of Figure 2 took place within the time interval from 2015 December 30 23:01 UT to 2015 December 31 00:31 UT and

included three consecutive plasma ejections, each of them had corresponding precursors. Finally, for the 23 investigated events a precursor was found in 20 cases. The detailed catalog of the investigated CJ parameters is presented in Table 1.

We investigated the statistical distributions of the precursor and the CJ individual parameters for both data set 1 and data set 2. We organized the parameters as follows (Table 2): (i) The precursor ignition duration (τ_{PI}), representing the half-width of the Gaussian fit to the first disturbance in the precursor. The τ_{PI} contains the information about the temporal properties of the precursor sources that enables us to judge the particular periods of the initially ignited disturbances. It should be noticed that some precursors consist of a single peak disturbance and in such cases the ignition and total duration of the precursors are co-measurable. In other

Table 2
Parameters Average Values CJs and Their Precursors

Parameters x	Maximum Probability f_0	Expected Value $\bar{x}$	σ (Variance)	Error $= \sigma/\sqrt{N}$
τ_{PI}	0.21/0.22	2.77/2.85	1.35/1.29	$\pm0.28/\pm0.27$
τ_{PT}	0.13/0.15	5.95/5.92	4.26/4.09	$\pm0.89/\pm0.85$
$\Delta\tau_{Peaks}$	0.12/0.11	10.25/10.13	6.83/7.59	$\pm1.43/\pm1.58$
τ_{CJ}	0.18/0.18	8.52/8.62	4.03/4.28	$\pm0.84/\pm0.89$
I_{CJ}/I_{PI}	0.31/0.28	2.18/2.59	0.80/1.12	$\pm0.17/\pm0.23$
τ_{CJ}/τ_{PI}	0.17/0.19	2.02/1.69	1.16/0.95	$\pm0.24/\pm0.20$
$\Delta\tau_{Peaks}/\tau_{PI}$	0.23/0.20	2.72/2.56	1.38/1.69	$\pm0.29/\pm0.35$
$\Delta\tau_{Peaks}/\tau_{CJ}$	0.16/0.16	1.36/1.34	0.67/0.67	$\pm0.14/\pm0.14$
Min. osc. period	…	1.24	0.83	±0.18
Max. osc. period	…	2.77	1.34	±0.30

Note. The CJ and corresponding precursor parameters with related variance and error estimations. τ_{PI} represents the precursor ignition duration; τ_{PT} is the precursor total evolution time span; (τ_{CJ})—CJ durations, $\Delta\tau_{Peaks}$—the time intervals between precursor and CJ peaks. All the quantities in the top four rows are measured in minutes and in the bottom four rows all are dimensionless. All values are given in accordance with the order data set 1/data set 2. In the two bottom rows, values are calculated only for data set 2.

cases, however, the precursors include an oscillatory-like behavior, and in this case, the total length of the process is significantly larger than the ignition (see Table 1). (ii) The precursor total evolution time span (τ_{PT}) showing how long the precursor process lasts before the jet outflow starts. There is another parameter also enabling us to judge time spans between the precursors and the CJs. (iii) The time intervals between precursor and CJ peaks ($\Delta\tau_{Peaks}$). (iv) CJ durations (τ_{CJ}) calculated in a similar way as the precursor ignition, as described above. We also evaluated the interrelation between the precursors and CJs by introducing the following dimensionless parameters: (1) the ratio of the coronal jet and precursor ignition peak intensities (I_{CJ}/I_{PI}) (the parameter manifests the rate of the coupling and the energy pumping from the precursor, and maybe some external source, to the main jet) and (2) their durations (τ_{CJ}/τ_{PI}). Finally, the ratio of the temporal gap between the precursor ignition and the jet peaks over (3) the precursor ignition ($\Delta\tau_{Peaks}/\tau_{PI}$) and (4) jet ($\Delta\tau_{Peaks}/\tau_{CJ}$) durations.

4. Discussion and Conclusions

We performed a statistical analysis of the brightness evolution of 23 small-scale jetlike events located within on-disk CHs. We studied the corresponding bright-point brightness average intensity evolution in time, using high temporal and spatial resolution SDO/AIA 193 Å images. We found that the vast majority of CJs are accompanied by a minor increase in mean intensity occurring several minutes before each intensive jet ejection. The precursor was identified in 20 out of 23 cases. We consider such enhancements of brightness as precursors of CJs. This result allows us to conclude that the presence of the precursor is a systematic property of CJs and the absence of the precursor in 3 of the 23 considered cases might be due to either incompleteness of the observational data. Alternatively, this can also be caused by the overlap between the precursor (τ_{PI}) and the jet (τ_{CJ}) duration intervals, which can happen when both are larger than the characteristic time between the peaks ($\Delta\tau_{Peaks}$) (zero values in corresponding fields). Despite the fact that there are some studies of the BP brightness evolution, for instance by Pucci et al. (2012), we performed introduction of the notion of CJ precursors.

According to our observation, the average lifetime of all examined τ_{PI} is 2.77/2.85 minutes, the mean ratio of CJ and precursor ignition peak intensities (I_{CJ}/I_{PI}) is 2.18/2.59, the average time between CJ and its precursor ($\Delta\tau_{Peaks}$) is 10.25/10.13 minutes, while the duration of the CJs (τ_{CJ}) is 8.52/8.62 minutes (see Table 2), which is in good agreement with other observational indications (see, e.g., Schmieder et al. 2013 and references therein). These parameters allow drawing preliminary conclusions on the observed processes. (i) We made an estimation of the mean maximum oscillation period by introducing the parameter τ_{PI} and also trough the FFT analysis. As we can see from the table, both estimations coincide very well. (ii) The relation between the total (τ_{PT}) and ignition (τ_{PI}) durations of the precursor shows that the longest period oscillation makes on average 2–3 oscillations before the jet starts, which is also justified by the mean values of ratios $\Delta\tau_{Peaks}/\tau_{PI}$ and τ_{CJ}/τ_{PI}. (iii) The value of $\Delta\tau_{Peaks}/\tau_{CJ}$ demonstrates the fact that the mean period of the mode that is involved in the jet outflow must be larger than that of the one involved in the precursor. (iv) The ratio of I_{CJ}/I_{PI} proves that the amplitude of the jet mode is larger than that of the precursor, which perhaps indicates the presence of the wave mode nonequilibrium driving (entropy variations or shear flows). This kind of parameter analysis can be continued. However, we stop at this moment as further analysis ultimately requires mathematically rigorous modeling, which is planned in the near future (see the corresponding remarks below).

The key conclusion that can be drawn from our analysis is that we were able to detect quasi-periodical oscillations with characteristic periods from sub-minute up to 3–4 minute values (see Table 1 and Figure 3) in the BP brightness that precede the jets. The AIA cadence favors such detection. The basic claim that can be made at this stage of pure observational analysis is that along with the conventionally accepted scenario of BP evolution through new magnetic flux emergence and its reconnection with the initial structure of the BP and the CH, certain MHD oscillatory and wavelike motions can be excited and these can take an important place in the observed dynamics. One can even imagine that these quasi-oscillatory phenomena might play the role of links between different epochs of the CJ ignition and evolution. However, we do not

have at this moment rigorous information either on the nature of this quasi-oscillatory behavior or on the mentioned possible links with the standard evolutionary scenario of the BPs and CJs. We just give a rough estimation of characteristic periods by applying a standard FFT routine to the data. A complete understanding of this issues requires further analytical and perhaps even numerical modeling of the processes discovered here, and such investigations will become a matter of future more extensive studies. These are not compatible with the format of the present short Letter, which only aims at the announcement of the novel observational evidence. In other words, the goal is to establish a notion of the CJ and its precursor patterns. However, we can make some general qualitative indications on the observed oscillatory processes and their link with some theoretical background. The quasi-oscillatory variations of intensity can be an indication of the MHD wave excitation processes due to the system entropy variations (Shergelashvili et al. 2007) or density variations (Zaqarashvili & Roberts 2002; Shergelashvili et al. 2005). The observed mutual positioning of open and closed magnetic field structures indicates that there is very likely a sharp outflow velocity gradients at the edges between the open and closed field line regions. All these conditions suggest a sequence of local magnetic reconnection events that could be the source of MHD waves due to impulsive generation or rapid temperature variations (Shergelashvili et al. 2007), on the one hand, and shear flow driven MHD wave excitation, coupling, and dissipation (self-heating mechanism) processes (Shergelashvili et al. 2006) and explosive type strongly non-adiabatic overreflections in the shear flows (Gogoberidze et al. 2004), on the other hand. The results obtained in this Letter create a solid ground for further studies in this direction.

ORCID iDs

Salome R. Bagashvili ⓘ https://orcid.org/0000-0003-4105-8623
Bidzina M. Shergelashvili ⓘ https://orcid.org/0000-0001-7179-466X
Stefaan Poedts ⓘ https://orcid.org/0000-0002-1743-0651
Teimuraz V. Zaqarashvili ⓘ https://orcid.org/0000-0001-5015-5762
Maxim L. Khodachenko ⓘ https://orcid.org/0000-0001-7954-5131

References

Archontis, V., Tsinganos, K., & Gontikakis, C. 2010, A&A, 512, L2
Aulanier, G., Golub, L., DeLuca, E. E., et al. 2007, Sci, 318, 1588
Bagashvili, S. R., Shergelashvili, B. M., Japaridze, D. R., et al. 2017, A&A, 603, A134
Boerner, P., Edwards, C., Lemen, J., et al. 2012, SoPh, 275, 41
Canfield, R. C., Reardon, K. P., Leka, K. D., et al. 1996, ApJ, 464, 1016
Chandra, R., Mandrini, C. H., Schmieder, B., et al. 2017, A&A, 598, A41
Chandrashekhar, K., Krishna Prasad, S., Banerjee, D., Ravindra, B., & Seaton, D. B. 2013, SoPh, 286, 125
Gogoberidze, G., Chagelishvili, G. D., Sagdeev, R. Z., & Lominadze, D. G. 2004, PhPl, 11, 4672
Gu, X. M., Lin, J., Li, K. J., et al. 1994, A&A, 282, 240
Guo, Y., Démoulin, P., Schmieder, B., et al. 2013, A&A, 555, A19
Guo, Y., Démoulin, P., Schmieder, B., et al. 2014, RMxAC, 44, 45
Kumar, M., Srivastava, A. K., & Dwivedi, B. N. 2011, MNRAS, 415, 1419
Lee, E. J., Archontis, V., & Hood, A. W. 2015, ApJL, 798, L10
Lemen, J. R., Title, A. M., Akin, D. J., et al. 2012, SoPh, 275, 17
Magara, T. 2010, ApJL, 715, L40
Mandrini, C. H., Démoulin, P., van Driel-Gesztelyi, L., et al. 1996, SoPh, 168, 115
Moore, R. L., Cirtain, J. W., Sterling, A. C., & Falconer, D. A. 2010, ApJ, 720, 757
Nisticò, G., Bothmer, V., Patsourakos, S., & Zimbardo, G. 2009, SoPh, 259, 87
Nolte, J. T., Solodyna, C. V., & Gerassimenko, M. 1979, SoPh, 63, 113
Panesar, N. K., Sterling, A. C., Moore, R. L., & Chakrapani, P. 2016, ApJL, 832, L7
Paraschiv, A. R., Lacatus, D. A., Badescu, T., et al. 2010, SoPh, 264, 365
Pariat, E., Antiochos, S., & DeVore, C. R. 2012, in 39th COSPAR Scientific Assembly Abstract E2.4-2-1
Pariat, E., Antiochos, S. K., & DeVore, C. R. 2009, ApJ, 691, 61
Pariat, E., Antiochos, S. K., & DeVore, C. R. 2010, ApJ, 714, 1762
Pontin, D. I., Al-Hachami, A. K., & Galsgaard, K. 2011, A&A, 533, A78
Pucci, S., Poletto, G., Sterling, A. C., & Romoli, M. 2012, ApJL, 745, L31
Raouafi, N. E., Patsourakos, S., Pariat, E., et al. 2016, SSRv, 201, 1
Ryutova, M., Berger, T., Frank, Z., & Title, A. 2008, ApJ, 686, 1404
Savcheva, A., Cirtain, J., Deluca, E. E., et al. 2007, PASJ, 59, S771
Schmieder, B., Guo, Y., Moreno-Insertis, F., et al. 2013, A&A, 559, A1
Schmieder, B., Malherbe, J. M., Mein, P., et al. 1996, in ASP Conf. Ser. 111, Magnetic Reconnection in the Solar Atmosphere, ed. R. D. Bentley & J. T. Mariska (San Francisco, CA: ASP), 43
Sheeley, N. R., Jr., & Golub, L. 1979, SoPh, 63, 119
Shergelashvili, B. M., Maes, C., Poedts, S., & Zaqarashvili, T. V. 2007, PhRvE, 76, 046404
Shergelashvili, B. M., Poedts, S., & Pataraya, A. D. 2006, ApJL, 642, L73
Shergelashvili, B. M., Zaqarashvili, T. V., Poedts, S., & Roberts, B. 2005, A&A, 429, 767
Shibata, K., Ishido, Y., Acton, L. W., et al. 1992, PASJ, 44, L173
Shibata, K., Nakamura, T., Matsumoto, T., et al. 2007, Sci, 318, 1591
Shimojo, M., Shibata, K., Yokoyama, T., & Hori, K. 2001, ApJ, 550, 1051
Sterling, A. C., Moore, R. L., Falconer, D. A., et al. 2016, ApJ, 821, 100
Sterling, A. C., Moore, R. L., Falconer, D. A., & Adams, M. 2015, Natur, 523, 437
Strong, K. T., Harvey, K., Hirayama, T., et al. 1992, PASJ, 44, L161
Tian, H., Xia, L.-D., & Li, S. 2008, A&A, 489, 741
Yokoyama, T., & Shibata, K. 1995, Natur, 375, 42
Young, P. R. 2015, ApJ, 801, 124
Young, P. R., & Muglach, K. 2014a, PASJ, 66, S12
Young, P. R., & Muglach, K. 2014b, SoPh, 289, 3313
Zaqarashvili, T. V., & Roberts, B. 2002, PhRvE, 66, 026401